J. Fluid Mech. (2013), *vol.* 723, *pp.* 429–455. © Cambridge University Press 2013
doi:10.1017/jfm.2013.137

Wall turbulence without walls

Yoshinori Mizuno[1,‡] **and Javier Jiménez**[1,2,†]

[1]School of Aeronautics, Universidad Politécnica de Madrid, 28040 Madrid, Spain

[2]Centre for Turbulence Research, Stanford University, Stanford, CA 94305, USA

(Received 22 August 2012; revised 9 January 2013; accepted 1 March 2013;
first published online 16 April 2013)

We perform direct numerical simulations of turbulent channels whose inner layer is replaced by an off-wall boundary condition synthesized from a rescaled interior flow plane. The boundary condition is applied within the logarithmic layer, and mimics the linear dependence of the length scales of the velocity fluctuations with respect to the distance to the wall. The logarithmic profile of the mean streamwise velocity is recovered, but only if the virtual wall is shifted to a position different from the location assumed by the boundary condition. In those shifted coordinates, most flow properties are within 5–10 % of full simulations, including the Kármán constant, the fluctuation intensities, the energy budgets and the velocity spectra and correlations. On the other hand, buffer-layer structures do not form, including the near-wall energy maximum, and the velocity fluctuation profiles are logarithmic, strongly suggesting that the logarithmic layer is essentially independent of the near-wall dynamics. The same agreement holds when the technique is applied to large-eddy simulations. The different errors are analysed, especially the reasons for the shifted origin, and remedies are proposed. It is also shown that the length rescaling is required for a stationary logarithmic-like layer. Otherwise, the flow evolves into a state resembling uniformly sheared turbulence.

Key words: turbulence simulation, turbulent boundary layers, turbulent flows

1. Introduction

Wall-bounded turbulence is a problem with two separate length scales (Townsend 1976). The core flow scales with the flow thickness, which will be denoted by h, and the near-wall layer scales in wall units, which are defined in terms of the friction velocity u_τ and of the kinematic viscosity ν, and will be denoted by a '+' superscript. The scale separation is measured by the friction Reynolds number h^+. The interaction of the two scale ranges is believed to take place across an overlap layer, usually called 'logarithmic', in which the eddy sizes are approximately proportional to the distance to the wall, y.

The logarithmic layer is interesting for several reasons. At high Reynolds numbers, it supports the transfer of momentum, and drag, from the wall to the core flow, across a wide range of scales, but how the transfer is organized and how much interaction is

† Email address for correspondence: jimenez@torroja.dmt.upm.es

‡ Present address: Mechanical and Systems Engineering, Doshisha University, 1-3 Tatara Miyakodani, Kyotanabe City, 610-0394, Japan.

https://doi.org/10.1017/jfm.2013.137 Published online by Cambridge University Press

there between the inner and outer layers remain open questions. Theories range from those in which the logarithmic eddies are created at the wall and migrate away from it (Adrian, Mainhart & Tomkins 2000), to those in which the opposite it true (Hunt & Morrison 2000). Almost the only tentative consensus is that most of the energy- and momentum-carrying eddies of the logarithmic layer are 'attached', in the sense that they span the full distance from the wall to their maximum height (Townsend 1961). Recent surveys have been given by Adrian (2007), Smits, McKeon & Marusic (2011) and Jiménez (2012).

The first question addressed in this paper is how independent is the logarithmic layer from the wall and, in particular, whether a logarithmic layer can be maintained with no wall at all. Indications that it can be done come from rough- and smooth-wall boundary layers, in which the wall dynamics are very different, but the logarithmic layers are not (Townsend 1976; Perry & Abell 1977; Jiménez 2004; Bakken *et al.* 2005; Flores & Jiménez 2006; Flores, Jiménez & del Álamo 2007).

Our strategy will be to substitute the wall by an off-wall boundary condition that imposes on an interior wall-parallel plane a synthetic velocity field that mimics the flow at that wall distance. Our lowest-order assumption will be that it is enough to impose on the flow the right length scale, which we will assume to be proportional to y.

That proportionality was originally hypothesized as an asymptotic limit at very high Reynolds numbers, and used in the classical derivation of the logarithmic velocity profile (Millikan 1938), but it has been observed experimentally and numerically in spectra and correlations at relatively modest Reynolds numbers in pipes (Morrison & Kronauer 1969; Perry & Abell 1975, 1977; Bullock, Cooper & Abernathy 1978; Kim & Adrian 1999; Guala, Hommema & Adrian 2006; Bailey *et al.* 2008), and in channels and boundary layers (Tomkins & Adrian 2003; del Álamo *et al.* 2004; Hoyas & Jiménez 2006; Monty *et al.* 2007; Jiménez & Hoyas 2008). Families of flow structures representing the coarse-grained dissipation (del Álamo *et al.* 2006; Flores *et al.* 2007) and the momentum transfer (Lozano-Durán, Flores & Jiménez 2012) have also been isolated in channels, and shown to be geometrically self-similar, in the sense of being attached to the wall with dimensions that scale linearly with their heights.

Interestingly, the linear scaling of the eddy sizes extends beyond the traditional range of validity of the logarithmic mean velocity profile ($y/h < 0.15$; see Österlund *et al.* 2000), and holds approximately to at least $y/h \approx 0.4$ in many flows (Zanoun, Durst & Nagib 2003; del Álamo *et al.* 2004; Monty *et al.* 2007; Jiménez 2012). Minor corrections, such as the use of a virtual origin for the linear law, extend its validity even further (Mizuno & Jiménez 2011). Part of the reason why that similarity is not easily recognized in the mean velocity profile is that it is not complete. Eddies much smaller than the distance to the wall are essentially isotropic and form a local Kolmogorov cascade (Saddoughi & Veeravali 1994), and structures much longer or wider than the flow thickness span the whole boundary layer and do not change size as they approach the wall (Perry & Abell 1977; Jiménez 1998; Kim & Adrian 1999; del Álamo *et al.* 2004; Jiménez 2012). On the other hand, the wall-normal velocity, the tangential Reynolds stresses and the strongest spectral cores of the other velocity components can be readily recognized as scaling linearly with the wall distance (Perry & Abell 1977; Hoyas & Jiménez 2006; Jiménez & Hoyas 2008). We will define the logarithmic layer as the region in which the eddy sizes scale linearly with y, irrespective of the mean velocity profile, and it is that linear dependence that we will try to reproduce in our numerical experiments. The hope is that it will lead, by itself, to the establishment of a natural logarithmic layer.

https://doi.org/10.1017/jfm.2013.137 Published online by Cambridge University Press

The second goal of this paper is more practical. Direct numerical simulations (DNSs) are at present too expensive to deal with most flows of industrial interest. If we accept that the integral length of the energy-containing eddies in the logarithmic layer is proportional to y, while the smallest eddies are of the order of the Kolmogorov viscous scale, $\eta^+ \sim y^{+1/4}$ (see Tennekes & Lumley 1972, p. 159), the number of degrees of freedom in a cube of side h is proportional to

$$N_{DNS} \sim \int_0^{h^+} (h^+/\eta^+)^2 \, \mathrm{d}y^+ \sim h^{+5/2}, \tag{1.1}$$

which is slightly larger than the usual estimation, $h^{+9/4}$, because the inhomogeneity of the flow concentrates eddies near the wall. In fact, the number of degrees of freedom per unit of y is proportional to $(y^+)^{-1/2}$, which justifies the use of logarithmic-layer estimates for the length scales, instead of outer ones. Equation (1.1) is the lowest possible limit for the number of points required in a numerical DNS grid.

The usual strategy to avoid the Reynolds number dependence of the number of grid points is large-eddy simulation (LES), in which all eddies smaller than a given fraction of the integral length are modelled, and which, therefore, only requires a fixed number of degrees of freedom. It can be argued that any computational problem requiring a fixed number of points, even if it is large, will eventually be solved by the growth of computer power, while potentially unbounded problems require a theory. Unfortunately, the LES strategy fails in wall-bounded flows. Repeating the estimate in (1.1), using lengths of $O(y)$ for the smallest eddies to be computed, we get

$$N_{LES} \sim \int_{y_0}^{h} (h/y)^2 \, \mathrm{d}y \sim (h/y_0)^2, \tag{1.2}$$

where the integral is dominated by the lower limit y_0. In general, the integral in (1.2) should extend to the point at which the lengths stop being proportional to y, which is $y_0^+ = O(1)$, so that $N_{LES} = O(h^{+2})$. Although lower than (1.1), that estimate still prevents the practical application of LES to most practical wall-bounded flows (Jiménez & Moser 2000). Our second reason to study the logarithmic layer is to explore how to construct off-wall boundary conditions which could be applied at a fixed y_0/h, independently of the Reynolds number, thus reducing the LES estimate in (1.2) to $O(1)$.

The search for off-wall boundary conditions for LES is not new. A common approach is to combine the solution of the unsteady Reynolds-averaged Navier–Stokes (RANS) equations for the near-wall layer with a LES solver for the core flow and many variations exist. The simplest ones assume equilibrium in the near-wall layer and apply the logarithmic law locally (Deardorff 1970) or include partial contributions from the acceleration terms and other improvements (Wang & Moin 2002; Catalano *et al.* 2003). Recent reviews can be found in Piomelli & Balaras (2002) and Piomelli (2008). A common problem with those approaches is that, while they do a good job of simulating the near-wall layer, they tend to provide poor boundary conditions for the outer flow, because RANS does not simulate fluctuations. Although several cures have been proposed for the discontinuities that appear (Nikitin *et al.* 2000; Hamba 2003; Piomelli *et al.* 2003; Keating & Piomelli 2006), the problem remains unsolved. On the other hand, note that any off-wall boundary condition, however perfect, would eventually have to be coupled to some sort of two-layer model to approximate the mean velocity of the missing inner region.

https://doi.org/10.1017/jfm.2013.137 Published online by Cambridge University Press

A physical approach closer to the spirit of this paper is due to Podvin & Fraigneau (2011), who used a wall model based on proper orthogonal decomposition (POD) modes to predict the flow at the off-wall boundary. It works well in relatively low-Reynolds-number channels, but the POD modes must be known in advance.

Two other papers should be cited. Even if not exactly an off-wall strategy, Pascarelli, Piomelli & Candler (2000) suggested a multi-block technique in which small DNS blocks are created in the inner layer and used to tile the wall with identical copies to provide a boundary condition for the outer flow. Although our technique is very different, we also find spurious periodicities in the boundary conditions, and our results will be compared with theirs.

The final interesting experiment is that by Orlandi *et al.* (2003), who fed velocities from an independent rough-walled channel DNS into the wall of a smooth one, in an attempt to reproduce roughness effects. Although their technique is also completely different from ours, and their boundary conditions are applied at the physical wall, the use of artificial velocities in a wall-parallel plane is conceptually similar to ours.

This paper is organized as follows. The numerical method is described in § 2, with emphasis on the off-wall boundary condition. The resulting statistics, including the behaviour of the spectra and correlation functions is presented in § 3. The new boundary condition is applied to LES in § 4, which also tests the effects of some variations of the off-wall boundary conditions. Finally, the results are discussed and conclusions offered.

2. Numerical simulations

We consider an incompressible turbulent channel driven by a streamwise pressure gradient between two parallel planes located at $y = 0$ and $y = 2h$. The streamwise, wall-normal and spanwise coordinates and velocity components are, respectively, (x, y, z) and (U, V, W), P is the kinematic pressure and the density is fixed to unity and dropped from the equations. Lowercase letters denote fluctuations with respect to the average $\overline{(\,)}$, defined over wall-parallel planes and time, and primed quantities denote root-mean-squared intensities, such as in $u'^2 \equiv \overline{u^2}$. Occasionally, the notation $(x_1, x_2, x_3) = (x, y, z)$ and $(u_1, u_2, u_3) = (u, v, w)$ will be used for convenience.

The flow is assumed to be spatially periodic in the two wall-parallel directions, with wavelengths L_x and L_z, and the simulation only considers the layer between two interior numerical boundaries at $y = y_b$ and $y = 2h - y_b$, with $0 < y_b < h$. The Navier–Stokes equations are solved for the primitive variables, U, V, W and P, using a fractional-step method similar to that of Simens *et al.* (2009) for boundary layers, although, in this case, the streamwise periodicity makes the generation of inflow and outflow conditions unnecessary. The spatial discretization is de-aliased collocated Fourier in the two wall-parallel directions, and fourth-order compact finite differences on a non-uniform staggered grid along y. The temporal integration is third-order Runge–Kutta with implicit marching for all of the viscous terms (Spalart, Moser & Rogers 1991). The Fourier modes of a generic variable ψ are $\widehat{\psi}(k_x, y, k_z; t)$, where k_x and k_z are wavenumbers in the streamwise and spanwise directions. We will also use wavelengths, defined as $\lambda_i = 2\pi/k_i$. The time t will generally be omitted, unless explicitly required by the argument at hand.

The definition of the simulations requires a velocity scale and a frame of reference. In traditional simulations, the latter is usually linked to the wall, while the velocity scale is either given as a fixed friction velocity or as a mass flux. In our case, the

https://doi.org/10.1017/jfm.2013.137 Published online by Cambridge University Press

absence of the wall makes the problem invariant to arbitrary Galilean transformations,

$$U_i \mapsto U_i + A_i(t), \tag{2.1}$$

including arbitrary accelerations, and there is no obvious preferred frame of reference. Neither can the mass flux, which depends on the frame velocity, be used to define the velocity scale. Our choice is to define: (i) the frame velocities A_i so that the instantaneous volumetric flux vanishes along the three directions; and (ii) the velocity scale by the fixed difference ΔU between the instantaneous velocities averaged over the wall-parallel planes at the centre and at the two numerical boundaries. In terms of the Fourier coefficients,

$$\widehat{U}(0, y_b, 0; t) = \widehat{U}(0, 2h - y_b, 0; t) = \widehat{U}(0, h, 0; t) - \Delta U, \tag{2.2}$$

with a similar condition for W (with $\Delta W = 0$). Continuity implies that the mean wall-normal velocity, $\widehat{V}(0, y, 0)$, is independent of y.

Fixing the fluxes requires uniform, but temporally fluctuating, pressure gradients that compensate the frame accelerations in the three directions, and which are computed by the pressure-correction substep at every time step. The two wall-parallel gradients are common to all simulations in which notionally infinite channels are approximated by spatially periodic domains. They are not usually included in the pressure statistics, because there is no well-defined spatial average for a secular pressure trend, and they are left out of the statistics below. The wall-normal pressure gradient is required to compensate the fluctuating normal Reynolds stress $\widehat{v^2}(0, y, 0)$ and the mean wall-normal acceleration. It is included in our pressure fluctuations, but is equivalent to that in standard channels, because the condition of zero wall-normal volumetric flux ensures that the mean wall-normal acceleration vanishes. The implementation of (2.2) is discussed in the next section, together with the rest of the off-wall boundary conditions.

2.1. *The off-wall boundary conditions*

The boundary conditions for the higher Fourier modes are constructed from the velocities in interior 'reference' planes $y = y_r$ and $y = 2h - y_r$, where $0 < y_b < y_r < h$, following a procedure conceptually similar to the method of Lund, Wu & Squires (1998) for creating inflow conditions for boundary layers using a downstream flow plane. Although the necessarily limited Reynolds numbers of our simulations make the existence of a true logarithmic layer questionable, the assumption will be that both y_b and y_r are in the self-similar range in which the flow length scales are proportional to the distance to the wall. As we noted in the introduction, that is approximately true over a reasonably wide range of wall distances, specially for the higher-Reynolds-number simulations. Only the operations on the lower boundary are described; those on the upper boundary are similar.

For each time step, the flow at y_r is first shrunk by a factor $\alpha = y_b/y_r$ to mimic the statistical proportionality of the length scales to the wall distance. Note that α^{-1} should be an integer to preserve the streamwise and spanwise periodicities of the flow. Next, to take into account the different advection velocities of the structures in the two planes, the rescaled velocity field is shifted in the two wall-parallel directions by amounts $\delta_j(t)$ determined by integrating the respective spatially averaged velocities,

$$\frac{\mathrm{d}\delta_j}{\mathrm{d}t} = \widehat{U}_j(0, y_b, 0) - \widehat{U}_j(0, y_r, 0), \tag{2.3}$$

https://doi.org/10.1017/jfm.2013.137 Published online by Cambridge University Press

where $j = 1$ or $j = 3$, and the initial $\delta_j(0)$ are chosen arbitrarily. In Fourier space, the shifting is done by multiplying each harmonic by the rotational factor $\exp(\mathrm{i}k_j\delta_j)$, as used, for example, in the simulations of uniformly sheared turbulent flows by Schumann (1985) and Jiménez (2007). The integration of (2.3) is performed in parallel to the Navier–Stokes equations, using an explicit Runge–Kutta. By combining the two manipulations, the mapping of the velocities from the reference plane to the boundary is

$$\widehat{\boldsymbol{U}}(k_x, y_b, k_z) = \widehat{\boldsymbol{U}}(\alpha k_x, y_r, \alpha k_z)\exp[\mathrm{i}\alpha(k_x\delta_x + k_z\delta_z)], \tag{2.4}$$

which is applied explicitly, with the boundary at time t_n synthesized from the reference information at time t_{n-1}. Special cases are the boundary conditions for the $(0, 0)$ Fourier modes, which represent the spatially averaged velocities and therefore require no phase shifting. They are also applied explicitly, using (2.2) to compute $U(0, y_b, 0; t_n)$ from $U(0, h, 0; t_{n-1})$.

Note that the delay by one time step is irrelevant because the two planes are effectively uncorrelated. The reason is two-fold. In the first place, two harmonic functions of different wavenumbers are orthogonal, and in the second place, the arbitrarily large phase shifts that develop over time mean that the information at the boundary is obtained from horizontally distant points of the reference plane. The integration times of our simulations are long enough for the two planes to move with respect to each other by several box lengths. As a consequence, the only role of the reference plane is to provide a physically realistic turbulent velocity to be used to synthesize the boundary condition. In addition, the length scale in the wall-normal direction can only be rescaled indirectly through the y-derivative of V, because continuity implies that,

$$\frac{\partial \widehat{V}}{\partial y}(k_x, y_b, k_z) = \alpha^{-1}\frac{\partial \widehat{V}}{\partial y}(\alpha k_x, y_r, \alpha k_z). \tag{2.5}$$

We will come back to those two points later. In our simulations the boundary and the reference planes are chosen so that $\alpha = 1/2$, which would imply that the synthesized boundary only has energy in the even-indexed Fourier modes; i.e. that the boundary plane is covered by a tiling of four identical sub-boxes. This is reminiscent of the simulations by Pascarelli *et al.* (2000), who used tiled minimal channels at the wall as boundary conditions for larger simulations above and found that the tiling periodicity was quickly lost in the flow interior. We will call that method D-scaling (from 'discrete', see figure 1*a*). To mitigate possible discreteness effects, a second method was implemented in which the energy of the Fourier wavenumber with indices (i_x, i_z) in $y = y_r$ is equally distributed in $y = y_b$ among the four neighbouring modes, $(2i_x, 2i_z)$, $(2i_x - 1, 2i_z)$, $(2i_x, 2i_z - 1)$ and $(2i_x - 1, 2i_z - 1)$. That method is called C-scaling (from 'continuous', see figure 1*b*), and is used in most simulations. The differences between the two schemes will be discussed in § 4, in the context of the application to LES.

We already noted in the introduction that, even at the relatively high Reynolds numbers of our simulations, the proportionality of the flow scales with the wall distance only applies to structures of intermediate sizes. Fluctuations of order h, which are especially strong for the streamwise velocity component, span the full channel without changing their wall-parallel dimensions (Perry & Abell 1977; Jiménez 1998; Kim & Adrian 1999; del Álamo *et al.* 2004). Those larger motions are not well-represented near the boundary by the linear rescaling in (2.4), and neither can their advection velocities be approximated by the local mean velocity (del Álamo &

https://doi.org/10.1017/jfm.2013.137 Published online by Cambridge University Press

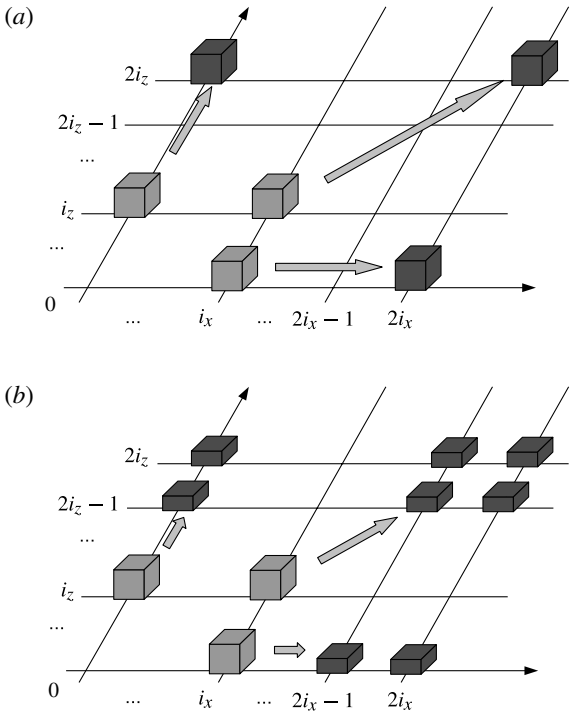


FIGURE 1. (*a*) D- and (*b*) C-rescaling. Light- (dark-) grey pillars represent the intensities of the Fourier modes in the original (rescaled) velocity field in the plane of Fourier indices (i_x, i_z).

Jiménez 2009). In spite of that, equation (2.4) is used for all wavenumbers in the experiments in this paper.

It is also known that the mean-squared fluctuations of the wall-parallel velocities increase logarithmically towards the wall (Townsend 1961; Jiménez & Hoyas 2008; Hultmark *et al.* 2012), so that their energies should not be the same at $y = y_b$ and y_r. Our boundary condition does not take that trend into account, because (2.4) makes the energies at both planes equal. We will see below that the result is a spurious 'bump' in the intensities near the boundary, but the effect is small. For example, it follows from the work of Townsend (1961), Jiménez & Hoyas (2008) and Hultmark *et al.* (2012) that the streamwise energy, which is $u'^{2+} \approx 6$ near the boundary, grows by about $\Delta u'^{2+} \approx 0.8$ over a factor of two in y, and it will be seen in § 3.2 that the correct logarithmic trend is recovered by the simulation within a very short distance from the boundary. Any technological application of the boundary conditions described here should probably include more realistic treatments of all of those aspects, but those adjustments would also introduce new parametrizations and modelling compromises. We have preferred to keep our boundary condition as simple as possible in the present proof-of-principle calculations, whose main purpose is to determine the ingredients that a synthetic condition should include to reproduce a logarithmic-like behaviour.

2.2. *Wall-less simulations*

The simulations discussed in this paper are summarized in table 1. There are two 'wall-less' DNSs and two 'wall-less' LESs in medium-sized computational boxes,

https://doi.org/10.1017/jfm.2013.137 Published online by Cambridge University Press

https://doi.org/10.1017/jfm.2013.137 Published online by Cambridge University Press

	L_x/h	L_z/h	y_b/h	y_r/h	Δ_x/η	Δ_y/η	N_x	N_y	N_z	$u_\tau T/h$	h^+	Rescale	Symbol
W900C	4π	2π	0.1	0.2	3	1.6	1536	277	1536	12	858	C	△
W2600C	4π	2π	0.05	0.1	4	1.7	3072	569	3072	11.5	2570	C	○
WLESC	4π	2π	0.05	0.1	32	3.2	384	307	384	37	2430	C	□
WLESD	4π	2π	0.05	0.1	32	3.2	384	307	384	38	2420	D	◇
WLESNR	2π	π	0.05	0.1	—	—	192	307	192	—	—	—	—
C950	8π	3π	—	—		(del Álamo *et al.* 2004)					934	—	▲
C2000	8π	3π	—	—		(Hoyas & Jiménez 2006)					2003	—	●

TABLE 1. Parameters of the simulations. The grid resolutions, Δ_x and Δ_y, are given in terms of the Kolmogorov scale η in the vicinity of the off-wall boundary. In all cases, $\Delta_z \approx \Delta_x/2$. The time interval used to compile statistics is denoted by T, normalized with the large-eddy turnover time h/u_τ. The 'rescale' column indicates the way to generate the boundary condition. The spacial resolution of the LES is given in terms of the Kolmogorov scale in W2600C. See the text for other symbols.

using the off-wall boundary technique just described. They are compared with standard 'full-channel' simulations at similar Reynolds numbers, C950 (del Álamo *et al.* 2004) and C2000 (Hoyas & Jiménez 2006). The two wall-less DNSs, W900C and W2600C, use C-rescaling, while the two wall-less LESs, WLESC and WLESD, in addition to assessing the applicability of the method to LES, test the differences between the continuous and discrete rescaling methods.

In addition, we performed simulations in smaller boxes to investigate specific points. They will be briefly discussed when dealing with the particular issues for which they were intended, but are not included in table 1.

More interestingly, we tested the off-wall boundary condition (2.4) without the rescaling step, i.e. using $\alpha = 1$. The results were similar to a uniformly sheared flow, with both the length scales and the intensities growing monotonically in time, strongly suggesting that the spatial stratification of the length scales is a necessary ingredient for the existence of a logarithmic region in wall-bounded flows. A LES illustrating that point will be discussed in § 4.

3. Statistics

3.1. *The mean velocity profile*

The mean streamwise velocities $\overline{U}^+$ of the wall-less DNSs are shown in figure 2(*a*), compared with the corresponding full channels. Owing to the Galilean ambiguity of the wall-less cases, all of the profiles are presented in defect form, referenced to the velocity at the centreline, $\overline{U}_c^+$. A further uncertainty is the magnitude of the friction velocity u_τ, because the wall-less simulations have no physical wall. For the purpose of this figure, u_τ is estimated by extrapolating the total shear-stress, $\nu\,\mathrm{d}\overline{U}/\mathrm{d}y - \overline{uv}$, to the notional position of the wall at $y = 0$ (see figure 2*c*). The friction Reynolds numbers given in table 1 for the wall-less channels are computed in that way.

It is clear from figure 2(*a*) that the mean velocity profile of the wall-less channels is steeper than in the full ones, as if the wall were closer to the numerical boundary, $y = y_b$, than to the position, $y = 0$, assumed by the boundary condition. The difference is clearer in figure 2(*b*), which displays the mixing length,

$$\ell(y) \equiv \left(\frac{\mathrm{d}\overline{U}^+}{\mathrm{d}y} \right)^{-1}, \tag{3.1}$$

the slope of which should be the Kármán constant κ (Mizuno & Jiménez 2011). In all cases, the profiles of ℓ are linear, with broadly similar slopes, but the wall-less channels are shifted downwards, which is the reason for the steeper velocity profiles in figure 2(*a*). The intercept of the mixing length with $\ell = 0$ can be interpreted as a virtual origin for the logarithmic velocity profile, and it is clear from figure 2(*b*) that the virtual origins of the wall-less cases are not at $y = 0$. A more reasonable approximation is

$$\ell = \kappa (y - y_{off}), \tag{3.2}$$

which integrates to

$$\overline{U}^+ = \kappa^{-1} \log(y^+ - y_{off}^+) + B, \tag{3.3}$$

where B is an additive constant. Shifted logarithmic approximations to the mean velocity profile of wall-bounded flows have been discussed before (Duncan, Thom &

https://doi.org/10.1017/jfm.2013.137 Published online by Cambridge University Press

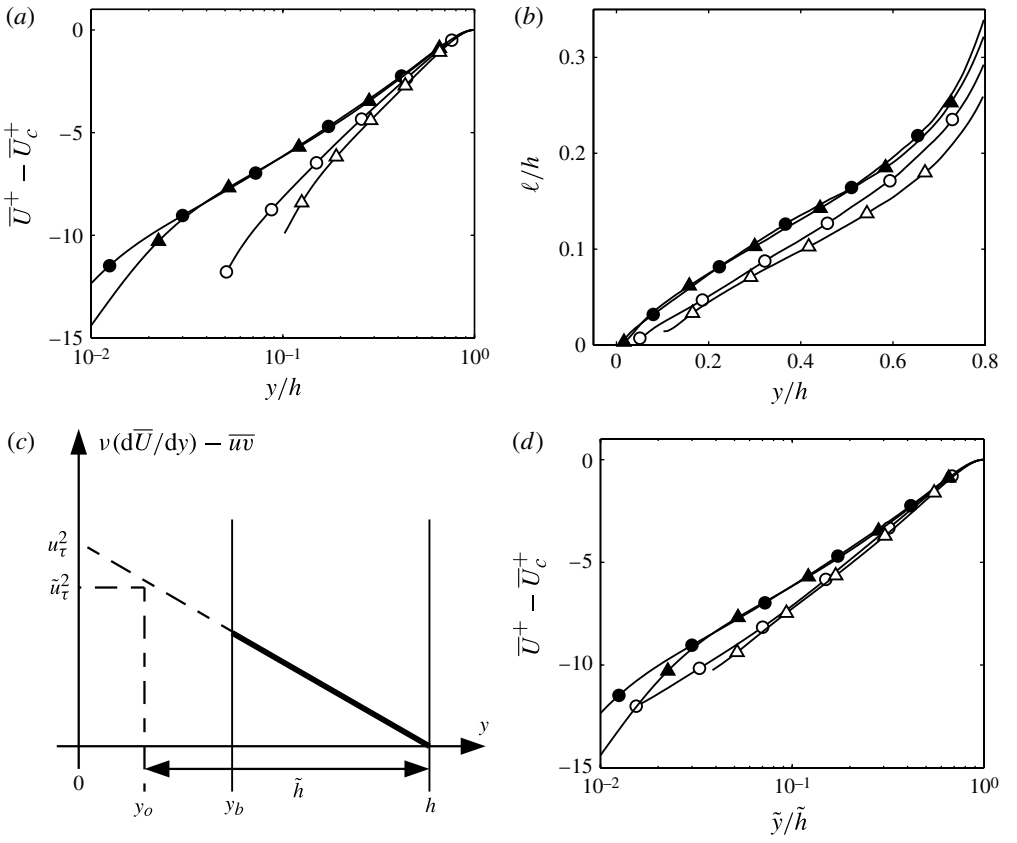


FIGURE 2. (*a*) Mean streamwise velocity $\overline{U}$ for W900C, W2600C, C950 and C2000. (*b*) Mixing lengths corresponding to the profiles in (*a*). (*c*) Sketch of the computation of the rescaled friction velocity and channel width, (*d*) as in (*a*), in rescaled coordinates. Symbols as in table 1.

Young 1970; Wosnik, Castillo & George 2000; Oberlack 2001; Buschmann & Gad-el-Hak 2005; Spalart, Coleman & Johnstone 2008). The offset represents the effect of the near-wall viscous layer on the logarithmic law, which cannot be extended to $y = 0$. Mizuno & Jiménez (2011) developed a systematic procedure to estimate the optimum parameters for (3.3). They applied it to several canonical data sets, both numerical and experimental, and found that the Kármán constant and the virtual origin depend on the type of flow and on the Reynolds number, although their results suggest that $y_{off}^+ \to 0$ at large h^+.

The parameters estimated for the flows in this paper are given in table 2, where it is clear that the wall-less cases differ from the full channels and that their virtual origins fall between the notional wall and the boundary plane. The most obvious interpretation is again that they represent the effect of the artificial boundary conditions on the logarithmic law, which cannot be expected to hold below y_b. They suggest that a rescaled shifted coordinate might give a better agreement between the two types of simulations. If we interpret the non-zero virtual origins of the full channels as a Reynolds number effect, we can define a 'baseline' shift, $y_f = y_{off}(\mathrm{DNS})$, which is only a function of h^+ (see figure 5 of Mizuno & Jiménez 2011), and define rescaled

https://doi.org/10.1017/jfm.2013.137 Published online by Cambridge University Press

	W900C	W2600C	WLESC	WLESD	C950	C2000
y_b^+	86	128	122	124	0	0
y_{off}^+	32	76	76	81	−29	−13
κ	0.28	0.33	0.31	0.32	0.35	0.36
y_o^+	51	87	86	90	0	0
$y_b^+ - y_o^+$	27	34	29	26	0	0
$\widetilde{u}_\tau/u_\tau$	0.97	0.98	0.98	0.98	1	1

TABLE 2. Offsets, virtual origins and Kármán constants for the fitted mean streamwise velocity profiles. See the text for details.

coordinates for the wall-less cases designed to make them comparable to the full ones. Considering for this purpose that the wall-less and full simulations in table 1 have similar h^+, we define

$$\widetilde{y} = y - y_o, \quad \widetilde{h} = h - y_o, \quad \widetilde{u}_\tau = u_\tau \,(\widetilde{h}/h)^{1/2}, \tag{3.4}$$

with

$$y_o = (y_{off} - y_f)/(1 - y_f/h), \tag{3.5}$$

where y_f is the virtual origin of the corresponding full flow with a similar Reynolds number. Those definitions are chosen so that $\widetilde{y} = \widetilde{h}$ when $y = h$, and $\widetilde{y}_{off}/\widetilde{h} = y_f/h$. Note that the new virtual wall, $\widetilde{y} = 0$ corresponds to $y = y_o$ and that $\widetilde{y} \equiv y$ in full channels. The modified friction velocity $\widetilde{u}_\tau$ is obtained by interpolating the linear shear-stress profile to $y = y_o$ (see figure 2*c*). The velocity profiles of the two wall-less DNSs are plotted in term of the rescaled coordinates in figure 2(*d*) and agree with the full channels much better than in the original coordinates. The physical reason for this offset will be discussed in detail in § 3.3.

The values of y_o from (3.5) have been added to table 2, as well as the rescaled friction velocities, which differ very little from the uncorrected ones. The table shows that, while y_o changes among cases, the offset relative to the numerical boundary, $y_b - y_o$, is always approximately 30 wall units. Although not included in the table, we conducted several tests in smaller computational boxes, $(L_x, L_z) = (\pi, \pi/2)$, to explore how y_o depends on the choice of y_b and y_r, or on the C- or D-rescaling methods. In all cases, $y_b^+ - y_o^+ \approx 30$.

The reason will be discussed extensively later, but a simple interpretation could be that the flow reacts to the artificial boundary condition by creating a spurious 'buffer' layer, the role of which is to let the flow adapt to an inconsistent boundary. However, there are no signs of viscous effects near the boundary. The linear behaviour of the mixing length in figure 2(*b*) and the logarithmic profile of the velocity in figure 2(*d*) extend all of the way to the boundary, and we will see in the next section that the fluctuations are also inconsistent with a spurious layer in which viscosity becomes dominant.

A more likely explanation is that imposing a Dirichlet boundary condition that is essentially uncorrelated with the flow interior is felt by the equations as a virtual wall, although the turbulent character of the applied velocities prevents the formation of a regular buffer layer. In fact, none of the rescaled figures in this paper change too much if they are replotted with the virtual wall exactly at the boundary plane, $y_o = y_b$.

https://doi.org/10.1017/jfm.2013.137 Published online by Cambridge University Press

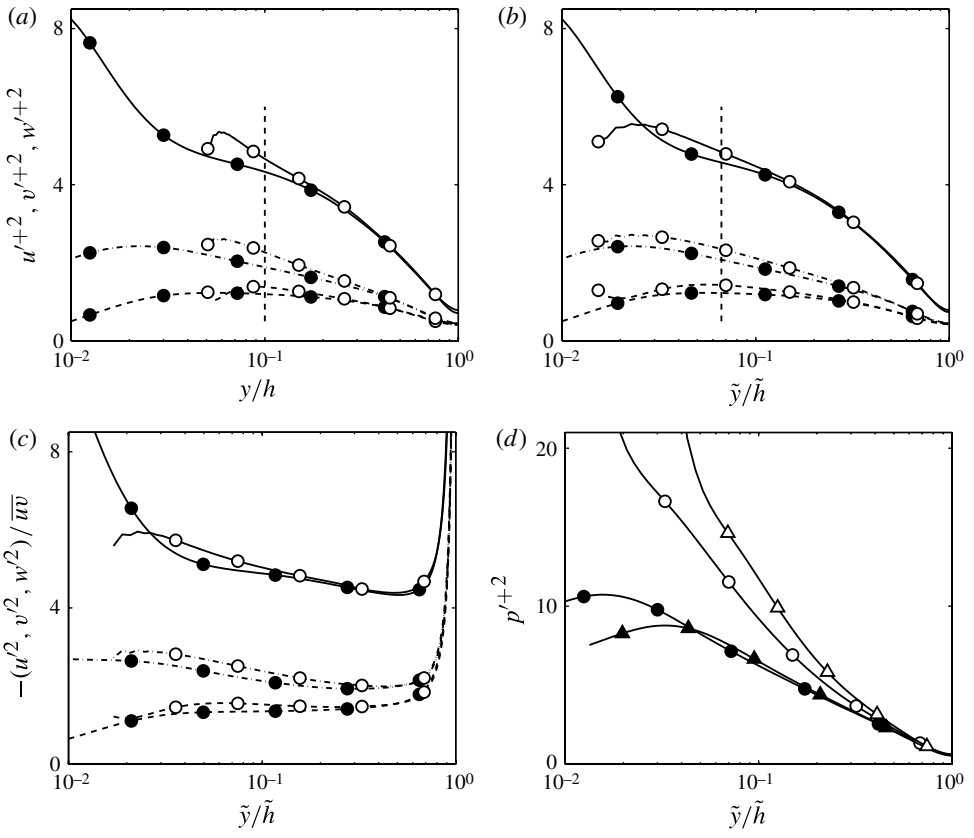


FIGURE 3. (*a*) Velocity fluctuation intensities for W2600C and C2000: u'^{+2}, w'^{+2} and v'^{+2} from top to bottom. (*b*) As in (*a*), in rescaled coordinates. The vertical lines in (*a*,*b*) are the position of the reference plane y_r. (*c*) As in (*a*), normalized with the local value of $\overline{uv}$. (*d*) Pressure fluctuations. Symbols as in table 1.

3.2. *Fluctuation intensities*

Figure 3(*a*) shows the intensities of the velocity fluctuations for C2000 and W2600C, which agree well above $y \approx 0.3h$, but which are slightly higher near the wall in the wall-less case. The same profiles are shown by figure 3(*b*) in terms of the rescaled coordinates (3.4), which improve the agreement substantially.

The wall-less channels have a weak maximum near the boundary, especially for u'^2 and w'^2, reminiscent of those observed in some 'detached-eddy' simulations and occasionally attributed to the formation of artificial buffer layers in the interface between the two models (Piomelli & Balaras 2002; Spalart 2009). As we mentioned in § 2.1, the most likely reason in this case is that the rescaling operation (2.4) redistributes the energy of the fluctuations in the reference plane to different wavenumbers at the boundary, but does not change the total energy. Therefore, the intensities at the reference plane and at the boundary are the same, while the intensity profiles grow logarithmically towards the wall, due to the progressive accumulation of inactive motions as the wall is approached (Townsend 1976, § 5.7). The logarithmic behaviour of w'^2 is clear in the figure, both for the full (Jiménez & Hoyas 2008) and for the wall-less cases. That of u'^2 is more easily seen in the wall-less channel, for

https://doi.org/10.1017/jfm.2013.137 Published online by Cambridge University Press

which the buffer-layer peak of the natural cases is missing. Its slope is intermediate between that found by Jiménez & Hoyas (2008) for channels when the largest scales are removed, $u'^{+2} \sim -1.15\log(y)$, and that found by Hultmark *et al.* (2012) for pipes at much higher Reynolds numbers, $u'^{+2} \sim -1.2\log(y)$. The spurious peak near the boundary can therefore be interpreted as the result of the recovery of the artificially low energy of the boundary to match the natural logarithmic trend in the interior of the flow, and it is interesting that it takes place within a very thin layer, of the order of $\Delta y^+ = 20$. The behaviour of the lower-Reynolds-number case W900C is similar to that just described.

Figure 3(*c*) tests that the amplitude differences in figure 3(*b*) are not due to the rescaling of the friction velocity in (3.4). Even when the intensities are normalized with the local Reynolds stress $-\overline{uv}$, removing the need for a velocity scale, the differences stay essentially the same as in figure 3(*b*). On the other hand, although not shown in the figure, the shifting of the wall distance is important. When figure 3(*c*) is plotted in terms of y/h, instead of $\widetilde{y}/\widetilde{h}$, the behaviour is closer to that in figure 3(*a*).

Note that, although figures 3(*a*)–3(*c*) show that the intensities of the wall-less channels are somewhat higher near the boundary than in the real case, their almost perfect agreement above $\widetilde{y}/\widetilde{h} \gtrsim 0.3$ suggests that this is a local consequence of the imperfectly synthesized boundary velocities. The reason can be traced to the pressure, whose fluctuation intensities are plotted in figure 3(*d*) for the four DNS channels. They are much stronger near the boundary in the wall-less cases than in the full ones, and stay strong at least for $\widetilde{y}/\widetilde{h} < 0.4$. Inspection of the pressure spectra (not shown) proves that all wavelengths get more intense, but that the effect is strongest for the smaller ones. For a given Fourier component, pressure satisfies a Poisson equation of the type

$$\frac{\partial^2 \widehat{p}_k}{\partial y^2} - k^2 \widehat{p}_k = \mathrm{RHS}, \tag{3.6}$$

where $k^2 = k_x^2 + k_z^2$ and the right-hand side (RHS) is a quadratic combination of basically all of the velocity derivatives (see, for example, Jiménez & Hoyas 2008). It has homogeneous solutions of the form $\widehat{p}_k \sim \exp(-ky)$, so that, if there is a source of strong velocity gradients near the boundary, its effect is only felt in a layer of order $\Delta y \sim \lambda/\pi = 2/k$. It follows from the way that our boundary condition is constructed that all of the wall-parallel velocity gradients are bounded, as well as $\partial_y v$ from continuity. The only two possible sources of high gradients are the wall-normal derivatives of the two wall-parallel velocities, which can be written in terms of the two wall-parallel vorticities. It can indeed be shown that both are too high at the boundary, where they share the lengths scales of the vorticity in general, of the order of $|\lambda^+| \approx 30\eta^+ \approx 70$ (Jiménez 2012). Therefore, their effect decays over a distance $\Delta y^+ \approx 20\,(\Delta y/h \approx 0.01)$ in W2600C, and they correspond to the very steep decay of the pressure fluctuations at the top left of figure 3(*d*). Those short fluctuations affect little the flow above y_r, but the somewhat larger ones that are seen in figure 3(*d*) decaying below $y/h \approx 0.4$ have a stronger effect. They can be traced to the mismatched v component at the boundary, which centres at wavelengths $|\lambda|/y_r \approx 1$–5 (see figure 5 below). That spurious pressure is unlikely to be avoided unless a 'softer' boundary condition can be formulated for the wall-normal velocity.

The energy budgets for the different velocity components are good indicators of how turbulence is maintained, and have been studied often from DNS data (Kim, Moin & Moser 1987; Mansour, Kim & Moin 1988; Hoyas & Jiménez 2008). The budgets for

https://doi.org/10.1017/jfm.2013.137 Published online by Cambridge University Press

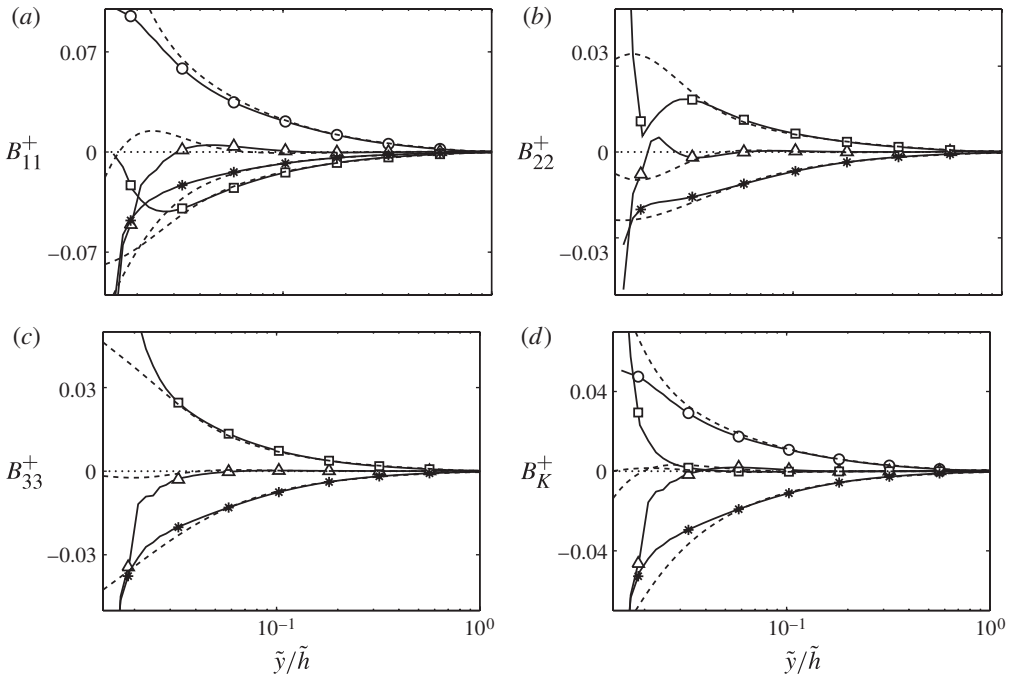


FIGURE 4. Budgets of the three diagonal components of the Reynolds stress tensor, (*a*) u'^2, (*b*) v'^2 and (*c*) w'^2, and (*d*) the kinetic energy density $K = (u'^2 + v'^2 + w'^2)/2$, as a function of $\widetilde{y}/\widetilde{h}$, for W2600C (——) and C2000 (– –). Symbols: ○, P_{ii}; △, T_{ii}; □, Π_{ii}; ∗, ϵ_{ii}. The horizontal dotted lines indicate zero. All of the terms are normalized in wall units.

the Reynolds stress tensor can be written as

$$\frac{\mathrm{D}\overline{u_i u_j}}{\mathrm{D}t} \equiv B_{ij} = P_{ij} + \epsilon_{ij} + T_{ij} + \Pi_{ij} + V_{ij}, \tag{3.7}$$

where the terms in the right-hand side of the equation are referred to as production, dissipation, turbulent diffusion, velocity-pressure gradient and viscous diffusion, respectively. They are defined by

$$P_{ij} = -\overline{u_i u_k}\,\overline{U}_{j,k} - \overline{u_j u_k}\,\overline{U}_{i,k}, \tag{3.8}$$

$$\epsilon_{ij} = -2\nu\,\overline{u_{i,k} u_{j,k}}, \tag{3.9}$$

$$T_{ij} = \overline{u_i u_j u_k}_{,k}, \tag{3.10}$$

$$\Pi_{ij} = -\overline{u_i p_{,j}} - \overline{u_j p_{,i}}, \tag{3.11}$$

$$V_{ij} = \nu\,\overline{u_i u_j}_{,kk}, \tag{3.12}$$

where subscripts after a comma $()_{,j}$ represent differentiation with respect to x_j. Repeated subscripts imply summation over 1–3. Figure 4 presents the comparison of the budgets of the three diagonal stresses and of the total kinetic energy in W2600C and C2000, as functions of $\widetilde{y}/\widetilde{h}$, normalized as $B_{ij}^+ = \nu B_{ij}/\widetilde{u}_\tau^4$. The viscous diffusion V_{ii} is omitted because it is negligible compared with the other terms. All of the budgets agree very well above $\widetilde{y}/\widetilde{h} \approx 0.05$ ($\widetilde{y}^+ \approx 100$), but differ near the boundary.

https://doi.org/10.1017/jfm.2013.137 Published online by Cambridge University Press

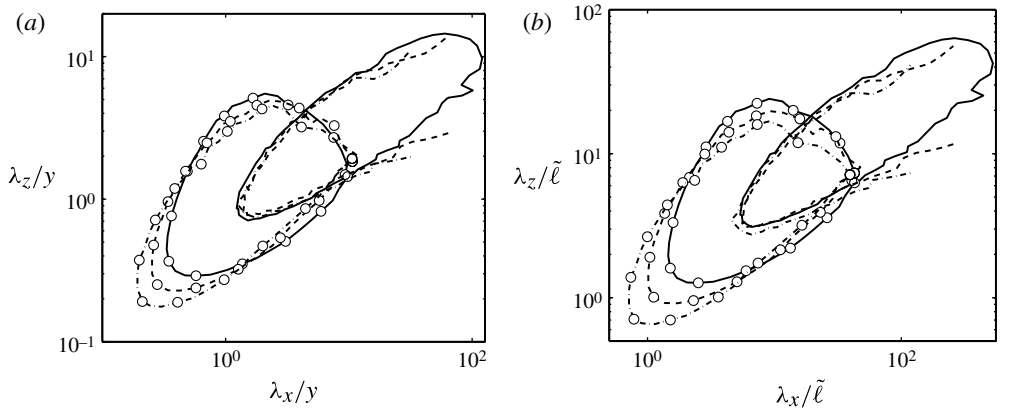


FIGURE 5. Premultiplied two-dimensional spectra, $k_x k_z \phi_{uu}$ (with no symbols) and $k_x k_z \phi_{vv}$ (with symbols), for W2600C at: ——, $y/h = 0.1$; – –, 0.2; – · –, 0.4. (*a*) As functions of λ_x/y and λ_z/y. (*b*) As functions of $\lambda_x/\tilde{\ell}$ and $\lambda_z/\tilde{\ell}$. Each spectrum is normalized by the mean-squared intensity of each component at each height and the contour level is 0.05.

The main differences are in the pressure and turbulent-diffusion terms, which are much stronger near the boundary of the wall-less channel than near the wall of the full simulation. In particular, note that the pressure term of the kinetic-energy balance in figure 4(*d*) is very strong near the boundary, while it essentially vanishes in the full simulation. The only pressure term in that equation is the pressure transport $\partial(pv)/\partial y$, which is small near walls because, even if the flow is very inhomogeneous there, the wall-normal velocity vanishes. That is not the case near the wall-less boundary, where the transpiration is high, and we have seen that the lack of coherence between the boundary and the overlying flow creates high pressures. Note also that this term transfers energy to the two transverse velocity components, but is not very important for the streamwise velocity, which is mostly inactive near the boundary. The extra energy created in this way is compensated by the turbulent diffusion of the extraneous eddies away from the wall.

3.3. *Length scales*

As we mentioned in the introduction, the length scales of the velocity fluctuations have been observed to depend linearly on y in attached turbulent flows, even beyond the classical range of the logarithmic velocity profile. Mizuno & Jiménez (2011) showed that the scaling range of moderately sized attached fluctuations can be extended even further by the use of the mixing length $\ell(y)$, to the point that it holds in $y^+ > 70$, $y/h < 0.5$ for Reynolds numbers as low as $h^+ \simeq 500$. The off-wall boundary condition (2.4) is intended to mimic that dependence, and it is interesting to inquire into whether ℓ, or its surrogate $\widetilde{y}$, represent well the length scales of the wall-less structures. A separate question is whether $\widetilde{y}$ can be used to improve the comparison between the two-point statistics of wall-less and full channels, even when a linear length scaling is not strictly satisfied.

The wall-parallel scales of the velocity fluctuations can be characterized by their two-dimensional spectra,

$$\phi_{ij}(k_x, y, k_z) \equiv \overline{\widehat{u}_i(k_x, y, k_z)\widehat{u}_j^*(k_x, y, k_z)}, \tag{3.13}$$

https://doi.org/10.1017/jfm.2013.137 Published online by Cambridge University Press

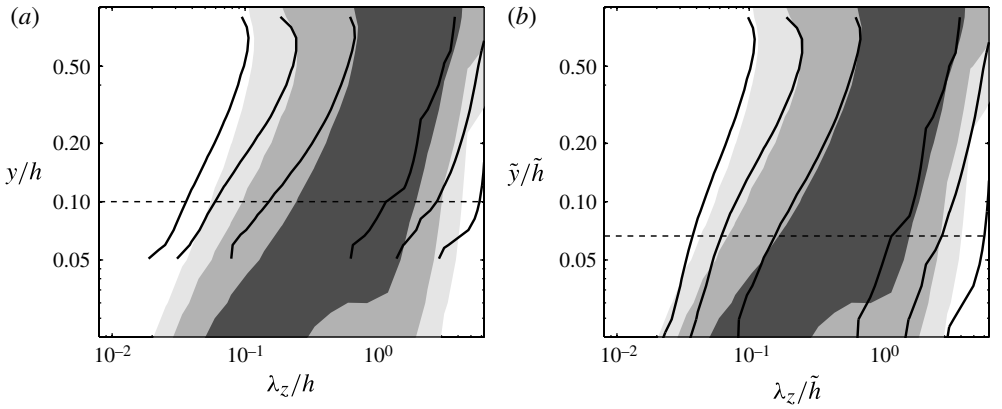


FIGURE 6. Premultiplied one-dimensional spectra $k_z\phi_{uu}$ for W2600C (lines) and C2000 (shaded), as a function of the spanwise wavelength and y. (*a*) Nominal coordinates. (*b*) Rescaled coordinates. The spectra are normalized by the mean-squared intensity at each height, and the contours are at 0.05, 0.1 and 0.22.

which are shown premultiplied in figure 5 for u and v in the wall-less channel W2600C. The Reynolds number of that simulation, and indeed of all of the simulations in this paper, is too high for y and ℓ to be significantly different (Mizuno & Jiménez 2011), and figure 5 shows that the two representations are difficult to distinguish above the reference plane. In that range, both work reasonably well, but the question persists of whether the wavelengths of the full and wall-less simulations collapse better overall if they are scaled with the distance y to the nominal wall or with the rescaled $\widetilde{y}$ or ℓ. Below y_r, the spectrum at the boundary is constructed by shrinking the reference plane by the ratio $y_r/y_b = 2$, and the nominal y is necessarily the correct choice, because the ratio of the corresponding rescaled coordinates for W2600C is $\widetilde{y}_r/\widetilde{y}_b \approx 3.9$. One could expect that the effect of the imposed y-scaling persists for some distance into the interior of the wall-less channel, but we saw in the previous sections that $\widetilde{y}$ does a better job of representing the mean velocity and fluctuation profiles everywhere, which suggests that the same could also be true for the spectral length scales.

The question is addressed in figure 6, which shows that, as in the case of the one-point statistics, $\widetilde{y}$ is also a better choice for the spectra. Note that, because $\widetilde{y}$ is designed to represent the mixing length in both simulations, figure 6 implies that the spectral lengths behave as the local velocity gradient, rather than as the distance to the wall.

Even in rescaled coordinates, the spectra in figure 6(*b*) disagree below $\widetilde{y}_r$, mainly for the wider scales with $\lambda_z \gtrsim \widetilde{h}/2$, showing that, even if the rescaling improves the agreement of most statistical quantities, the flow below the reference plane of the wall-less channels is still incorrect. Figure 7 shows that the scales involved are mainly long, $\lambda_x > 3\widetilde{h}$, corresponding to the global modes identified by del Álamo *et al.* (2004). We have already mentioned that those modes do not change scale as they approach the wall, while our boundary condition shortens and narrows them, and figure 7(*b*) shows that they are indeed depleted near the wall. On the other hand, the lack of large scales near the boundary does not seem to have a big effect above y_r, and the simplest way

https://doi.org/10.1017/jfm.2013.137 Published online by Cambridge University Press

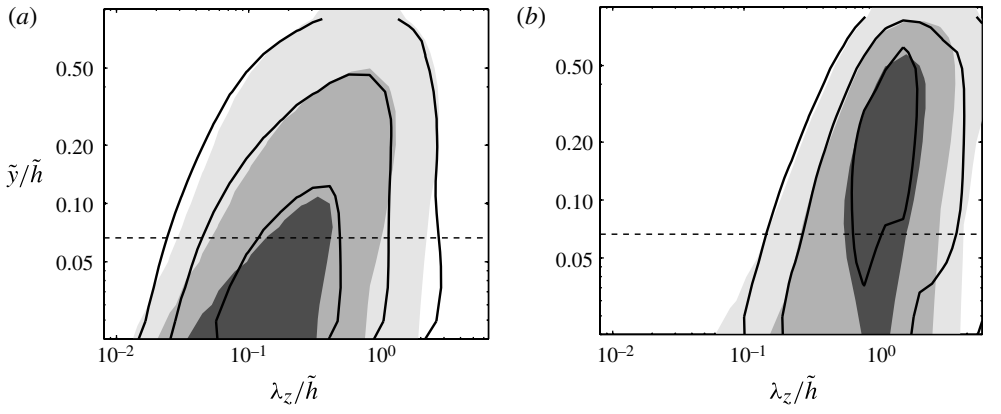


FIGURE 7. Premultiplied one-dimensional spectra $k_z\phi_{uu}$ for W2600C (lines) and C2000 (shaded), as functions of the spanwise wavelength and y. (*a*) For $\lambda_x < 3\widetilde{h}$. (*b*) For $\lambda_x > 3\widetilde{h}$. The spectra are normalized with $\widetilde{u}_\tau$, and the contours are at 0.1, 0.3 and 0.8.

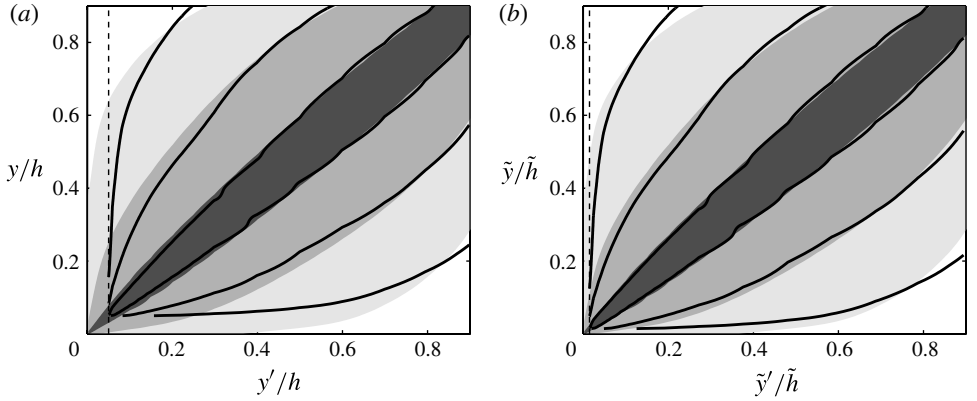


FIGURE 8. Autocorrelation $C_{uu}(y, y')$ for W2600C (lines) and C2000 (shaded), as a function of the y and y'. (*a*) Nominal coordinates. (*b*) Rescaled coordinates. The contours are 0.1, 0.3 and 0.7, and the dashed lines are the off-wall numerical boundary.

of summarizing the evidence up to this point is that the flow behaves as if the wall were located near the numerical boundary.

However, the largest discrepancy between the wall-less and full simulations, and the one that probably explains most of the observed differences, is revealed by figure 8, which shows the wall-normal correlation of the streamwise velocity,

$$C_{uu}(y, y') = \frac{\overline{u(y)u(y')}}{u'(y)u'(y')}. \tag{3.14}$$

The wall-normal correlations of the transverse velocity components, C_{vv} and C_{ww}, are known to scale linearly with y better than the spectra (Hunt *et al.* 1987; del Álamo *et al.* 2004). The linear scaling of C_{uu} fails because the global modes are coherent across the channel, but the strongest correlation levels, representing small detached structures, and correlations computed excluding the largest scales, also grow linearly

https://doi.org/10.1017/jfm.2013.137 Published online by Cambridge University Press

with y (Bullock *et al.* 1978). The failure of the global scaling of C_{uu} and the linear scaling of its stronger contours are clear in figure 8(*a*) for the full channel below $y \approx 0.3h$. The wall-less simulation behaves similarly to the full simulation far from the wall, but it separates from it near the boundary. Its correlation length drops almost to zero at $y = y_b$, whereas that only happens for the full channel in the immediate vicinity of the wall. The reason is almost surely that, as we have already mentioned, the phase shift and the rescaling introduced by the synthesizing step (2.4) destroys the coherence of the boundary plane with the flow above it. Figure 8(*b*) shows that the effect of the rescaled $\widetilde{y}$ is to restore the correct behaviour of the correlation length. The spanwise components C_{ww} (not shown) has weaker large-scale structures, but the effect of the boundary condition is the same as for C_{uu}; its correlation length at the boundary plane is closer to what it should be at the wall than to its correct value $y = y_b$. The wall-normal component C_{vv} behaves better, because its scales are controlled at the boundary by $\partial_y v$.

Note that this behaviour is different from those reported by Orlandi *et al.* (2003), who found that the most dangerous forcing was that by v, but their experiments involved imposing a single velocity component at a wall in which the other two components were set to zero. They therefore imposed no scale constraints different from those in a smooth wall, and the effect of their forcing was controlled by different mechanisms.

It is interesting to consider at this point what those observations imply for the question of which is the cause and which the effect of the similar behaviours of the correlation length and of the velocity profile. Mizuno & Jiménez (2011) showed that the spectral and correlation lengths scale better with $\ell \sim (\mathrm{d}\overline{U}/\mathrm{d}y)^{-1}$ than with the distance to the wall, which they interpreted as implying that the mean shear determines the scale. However, figures 6 and 8 show that their proportionality persists even when both, the length scale and the velocity gradient, are incorrect and, since it is clear that the shorter correlation lengths are caused in this case by the boundary condition (2.4), the strong implication is that the short correlation causes the steeper profile, instead of the other way around. A corollary would be that a better boundary condition should not only attempt to represent the wall-parallel spectral length scales, but the wall-normal ones as well.

4. Large-eddy simulations

We saw in the introduction that modelling of the inner layer is a central issue in reducing the computational requirements of the LES of wall-bounded turbulent flows, and one of the goals of this section is to investigate whether the boundary conditions developed above for DNSs can also be used for that purpose. Second, since the high-Reynolds-number direct simulations of the previous section are too expensive to allow extensive experimentation, we will use the cheaper LESs to investigate the question of C- versus D-scaling of the boundary spectra, and to demonstrate the importance of rescaling in maintaining an equilibrium flow.

Since our interest is in testing the boundary condition, rather than in optimizing LESs, we use a simple Smagorinsky (1963) subgrid model, in which the eddy viscosity ν_T is expressed in term of the filtered velocities $\breve{U}_i$, as

$$\nu_T = (C_S \Delta)^2 \, |\breve{S}|, \tag{4.1}$$

https://doi.org/10.1017/jfm.2013.137 Published online by Cambridge University Press

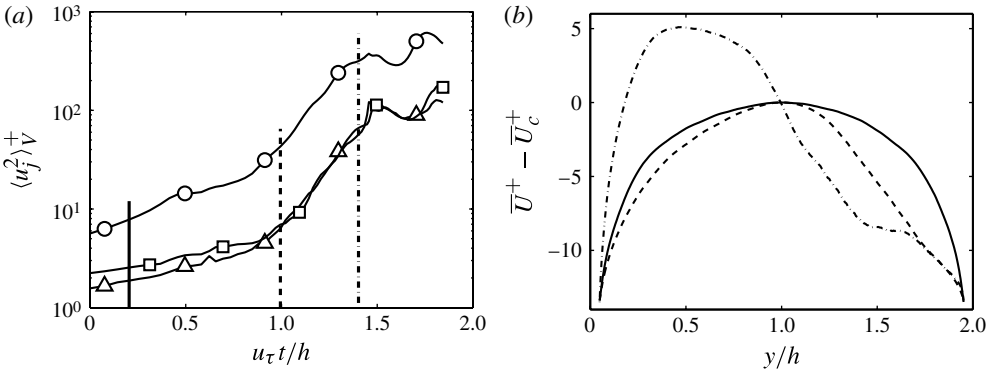


FIGURE 9. (*a*) Time evolution of the mean-squared velocity fluctuations averaged over the whole computational box: ○, u; △, v; □, w. (*b*) Spatially averaged velocity profile at the times indicated by the vertical lines in (*a*) with the corresponding line types. The friction velocity used for this case is from the statistically steady field used as initial condition.

where $C_S = 0.16$ is the Smagorinsky constant, $\Delta = (\Delta_x + \Delta_y + \Delta_z)/3$ is the filter width, $|\check{S}| = (2\check{S}_{ij}\check{S}_{ij})^{1/2}$, and

$$\check{S}_{ij} = \frac{1}{2}\left(\frac{\partial \check{U}_i}{\partial x_j} + \frac{\partial \check{U}_j}{\partial x_i}\right). \tag{4.2}$$

Consider first the necessity of rescaling. We mentioned in § 2 that enforcing the non-uniformity of the length scale with the distance to the wall is required to maintain a logarithmic layer. That was checked in small-scale simulations early in our investigation, since it is a central assumption of the whole procedure, and is illustrated here by the wall-less LES in figure 9, in which the boundary conditions are the same as in the other simulations, but no rescaling of the fluctuations takes place. Its parameters are listed as WLESNR in table 1. The initial condition is taken from a statistically steady C-rescaled LES, and the boundary conditions are switched at $t = 0$ to (2.4) with the rescaling ratio $\alpha = 1$. The initial condition for the phase offset in (2.3) is also reset to zero at that time. Figure 9(*a*) shows the time evolution of the volumetric averages of the velocity fluctuation intensities defined with respect to the instantaneous mean velocity profiles. They soon start to grow exponentially, as in the initial evolution of sheared turbulence (Champagne, Harris & Corrsin 1970; Rogers & Moin 1987), and only equilibrate at an energy level that is two orders of magnitude larger than the initial one, as in sheared flows whose length scales fill the computational box (Pumir 1996). At the same time, figure 9(*b*) shows that the mean velocity profile, $\widehat{U}(0, y, 0)$, changes radically and approaches a uniformly sheared flow. A truly uniform shear is inconsistent with (2.2), which requires that the mean velocities at the two boundaries should be equal and fixed with respect to that at the centreline, but the flow reacts by becoming asymmetric, approximating a uniform shear over most of the domain, and concentrating the opposite shear in a thin layer near the other wall. Although not shown here, the growth of the intensities takes place at large scales that are well resolved by the LESs.

Consider next the spectral rescaling method. We have already mentioned that our off-wall boundary condition, specially with discrete scaling, is conceptually similar

https://doi.org/10.1017/jfm.2013.137 Published online by Cambridge University Press

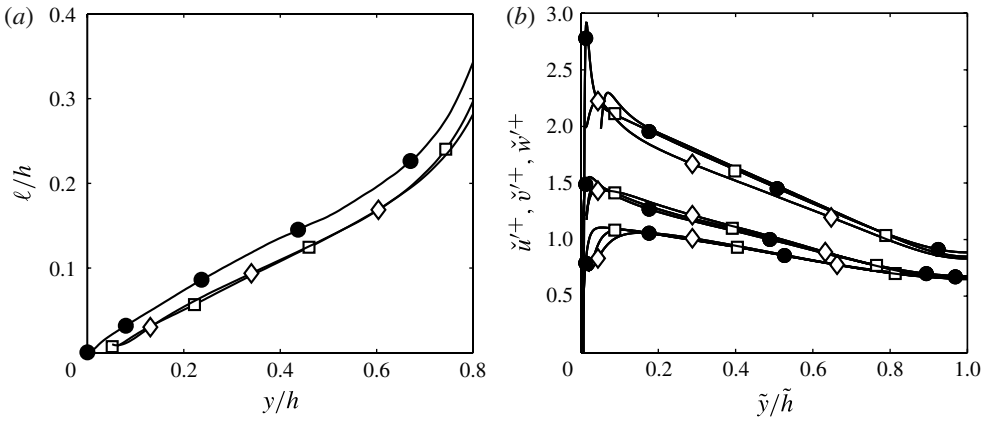


FIGURE 10. Comparison between the LESs, WLESC and WLESD, with the off-wall boundary and the full DNS channel C2000. (*a*) Mixing length ℓ. (*b*) Fluctuation intensities, $\check{u}'$, $\check{w}'$ and $\check{v}'$, from top to bottom. Symbols as in table 1.

to the experiments of Pascarelli *et al.* (2000), who proposed a multi-block LES technique in which the inner layer was substituted by periodic arrays of identical smaller units. Although that technique was intended as hierarchical, with several tiling levels spanning the resolution gap between the viscous wall layer and the flow core, their actual experiment in a subsonic time-developing boundary layer used a spanwise tiling of two minimal units, interfaced to a single overlying block. They reported that the tiling periodicity was lost in the central block and we will be interested in testing whether the same is true for our discrete D-scaling.

The two LESs in table 1, WLESC and WLESD, use C- and D-rescaling, respectively, but are otherwise identical to W2600C, including the molecular viscosity and the off-wall boundary condition. The number of grid points is reduced by approximately 1/120 with respect to W2600C, and there is no explicit filtering, except for the grid resolution Δ. As in the DNSs of the previous section, the mixing lengths determined from the $\overline{\check{U}}$ profiles of both LESs are best represented by offsets that move the virtual wall to the vicinity of the boundary plane (see figure 10*a*). Their fitting parameters are given in table 2, and are comparable to those for W2600C. Figure 10(*b*) compares the fluctuation intensities of the LESs with the unfiltered C2000, using the rescaled coordinate $\widetilde{y}/\widetilde{h}$. Both LESs agree with C2000 almost as well as the wall-less direct simulation W2600C, although the u' profile of WLESC is slightly better than WLESD. Note that the resolution of the present LESs is enough to capture all the energetic modes of the velocity fluctuations, which do not need to continue to be resolved as they shrink toward the viscous limit near the wall.

The energy budgets of the LESs (not shown) differ little from those of W2600C, except for the lower molecular dissipation reflecting the effect of the eddy viscosity. The main difference between the two LESs is a slightly stronger molecular dissipation in WLESC, persisting at the centre of the channel, which implies that the eddy viscosity and the resolved velocity spectra are different in the two cases. The dissipation by the subgrid model is 65 % of the total in WLESC and 75 % in WLESD.

Figure 11(*a*) and (*b*) show the premultiplied two-dimensional spectra of the streamwise velocity at $y/h = 0.3$ and 0.6, for WLESC, WLESD and W2600C. The smallest scales are missing from the two LESs at $y = 0.3h$, but the damping is stronger

https://doi.org/10.1017/jfm.2013.137 Published online by Cambridge University Press

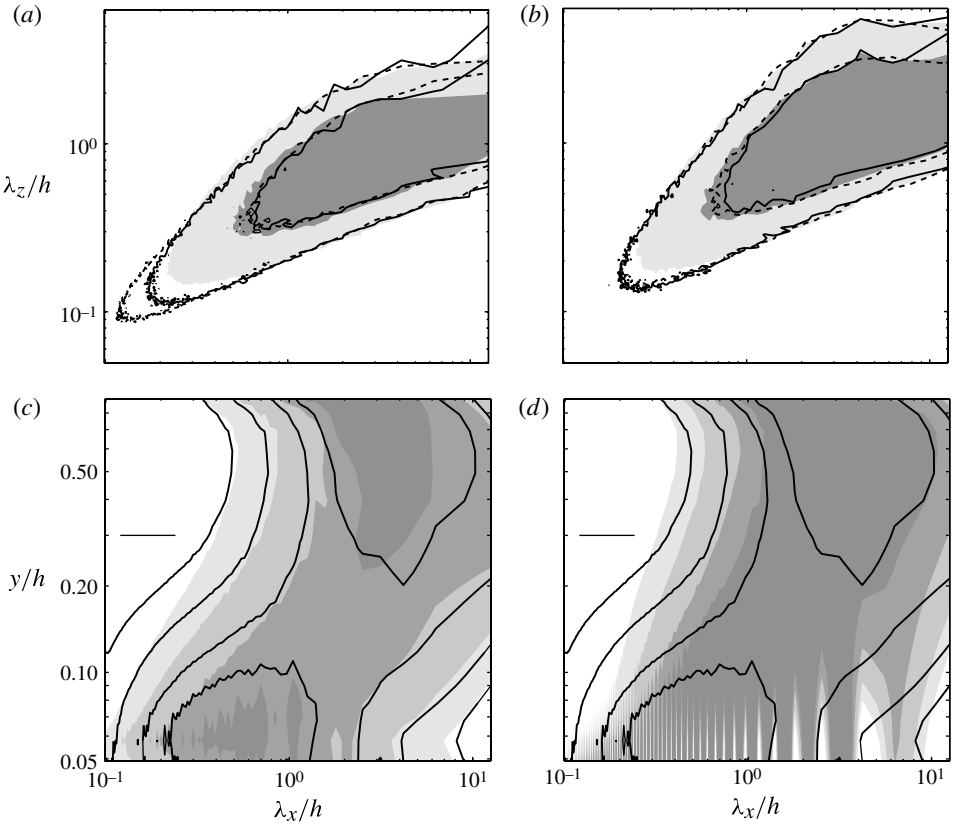


FIGURE 11. Comparison between the spectra of $\check{u}$ in LESs and DNSs, both using the off-wall boundary condition. (*a*) Premultiplied two-dimensional spectra normalized with $\check{u}_\tau^2$ at $y = 0.3h$: ——, W2600C; – –, WLESC; shaded, WLESD. Contours are 0.1 and 0.2. (*b*) As in (*a*), for $y = 0.6h$. Contours are 0.05 and 0.1. (*c*) One-dimensional premultiplied spectra as functions of λ_x and y, normalized at each height with the local intensity: ——, WLESC; shaded contours, W2600C. Contours are 0.1, 0.13, 0.17 and 0.2. (*d*) As in (*c*), but shaded contours are WLESD. The horizontal segments in (*c*,*d*) are a factor of two.

for WLESD. At $y = 0.6h$, essentially all of the scales are resolved in WLESC, but not in WLESD, which explains the discrepancy of the subgrid dissipations. The large scales agree well in the three cases.

The root of the difference is revealed in figure 11(*c*) and (*d*), which compare, respectively, the wall-normal evolutions of the one-dimensional longitudinal premultiplied *u*-spectrum of W2600C with those of WLESC and WLESD. Figure 11(*c*) shows that the spectra of W2600C and WLESC agree well, except for the expected lack of dissipative scales near the boundary. On the other hand, figure 11(*d*) shows that WLESD has more energy than W2600C around $\lambda_x/h = 1$–2, and less energy in the longer modes, where the discreteness of the boundary condition extends deeply into the channel.

Examples of instantaneous fields of u are shown in figure 12 for C2000, W2600C, WLESC and WLESD at $y = 0.6h$. Even at that relatively large distance from the wall, the flow structures are appreciably different in the D-scaled simulation. While

https://doi.org/10.1017/jfm.2013.137 Published online by Cambridge University Press

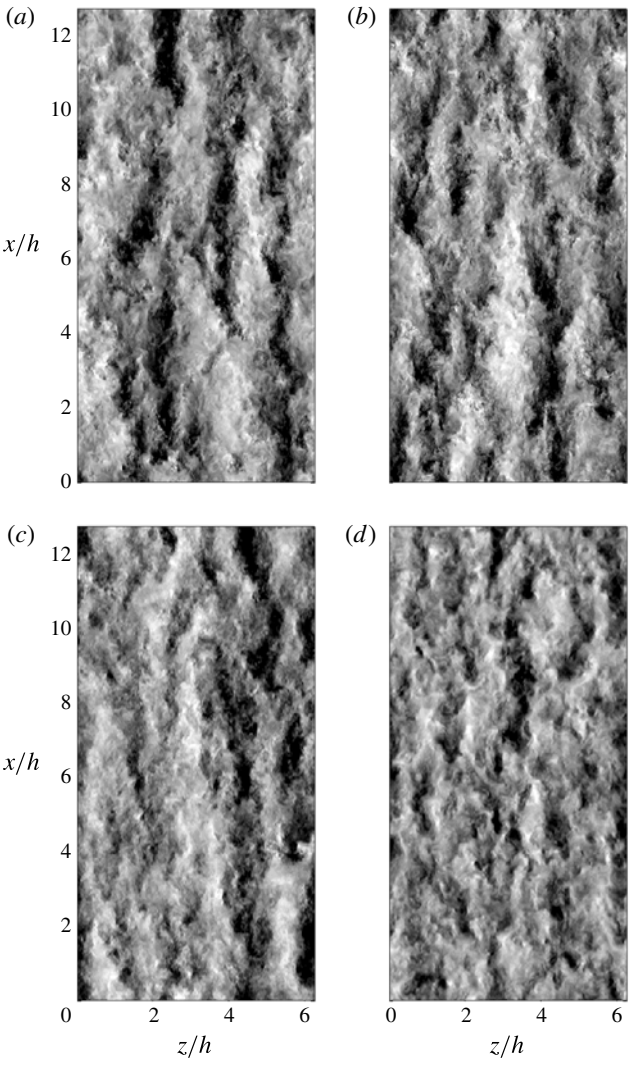


FIGURE 12. Instantaneous perturbation u fields for (a) C2000, (b) W2600C, (c) WLESC and (d) WLESD, for $y = 0.6h$. Mean flow is upwards. The shading changes from black below $-3u_\tau$ to white above $3u_\tau$.

W2600C and WLESC reproduce well the structures of the full channel, WLESD lacks the longest structures and the flow is visually shorter. Its structures are at most $2h$ long, while those in the other simulations span most of the box length ($\approx 10h$). The spanwise scales are similar in all cases.

Note that these results disagree with Pascarelli *et al.* (2000), although it is unclear whether the reason is our higher Reynolds number, the different type of flow, or some other detail of either simulation. The results also demonstrate that one-point statistics are not enough to judge the quality of simulations. Even when they are similarly reproduced by two simulations, the energy distribution, and the structural details, can be substantially different.

https://doi.org/10.1017/jfm.2013.137 Published online by Cambridge University Press

5. Discussion and conclusions

We have performed DNSs of turbulent channels in which the inner layer is replaced by an off-wall boundary condition where the velocities are substituted by a rescaled and shifted copy of an interior reference plane. The idea is to mimic the linear variation of the length scales of the flow with the wall distance, and it is remarkable that such a simple expedient results in a flow with a well-developed logarithmic layer. Tests in which the rescaling was not applied resulted in a flow much closer to homogeneous shear turbulence, showing that the scale variation is a necessary ingredient of wall-bounded turbulence. That has been illustrated above by a LES.

Since the off-wall condition is applied at wall distances usually associated with the lower logarithmic layer ($y/h = 0.05$, $y^+ = 130$), the flow lacks all of the structures usually present in the near-wall buffer layer, including the kinetic energy maximum. The mean velocity profile remains approximately logarithmic all of the way to the boundary, and so do the profiles of the velocity fluctuation intensities (Townsend 1976). Even the statistical properties of the structures defined by a strong Reynolds stress (Lozano-Durán *et al.* 2012) are essentially identical to those in full channels (A. Lozano-Durán, Personal communication). That is consistent with the results of Flores & Jiménez (2006) who found that the properties of vorticity clusters (del Álamo *et al.* 2006) change little when the buffer layer is manipulated to mimic rough flows. The present experiments modify the buffer layer even more profoundly (indeed, suppress it), and the Reynolds number ($h^+ = 2600$) is higher. They reinforce the conclusion that the logarithmic structures do not depend on seeding from the wall.

Because the present simulations lack a viscous sublayer, the resolution requirements are relaxed with respect to full DNSs. The resolution can be set in terms of the Kolmogorov viscous scale at the boundary, and does not need to resolve the wall. In our highest-Reynolds-number simulation, the savings in the y-grid are $\sim$40 %. In fact, we have shown that LESs at the same Reynolds number, using $\sim$100 times less points, give results essentially identical to the DNS.

On the other hand, the agreement with full-domain simulations is not complete. Most errors are local to the neighbourhood of the boundary, as can be expected from the accommodation region of any artificial boundary condition, but some of them extend deeper into the flow ($y/h \approx 0.3$–0.4). Of those, some can be easily avoided, such as the persistence of spurious periodicities introduced by the rescaling of the boundary velocity (D-scaling), which disappears after spectral smoothing of the boundary plane (C-scaling). Others are relatively mild, such as the 15 % overshoot of the velocity fluctuation intensities near the numerical boundary, or the depletion of the largest scales in the same region.

Two are more serious. The first is a strong increase of the pressure fluctuations near the boundary, which can be traced to the 'hard' Dirichlet boundary conditions imposed on the velocities. The extra pressure has two components. One is due to the small-scale wall-parallel vorticity created by the difference between the wall-parallel boundary velocities and the flow above. That component is very strong, but is restricted to the immediate vicinity of the boundary and can probably be taken into account by sacrificing the first few grid points of the simulation. A weaker component has wall-parallel scales of the order of the wall-normal velocity and extends deeper into the channel. The wall-normal velocity is copied into the boundary from the interior reference plane without any effort to guarantee continuity and it is left to the pressure to resolve any inconsistency between the boundary transpiration velocity and those induced by the overlying structures. The extra pressure fluctuations thus induced modify some of the terms of the energy budgets near the boundary and account for

https://doi.org/10.1017/jfm.2013.137 Published online by Cambridge University Press

the modest increase of the velocity fluctuations in that region. Any improvement of the present procedure should include a 'softer' boundary condition for the pressure.

The second problem is that the mean velocity profile, and most other flow properties, behave as if the wall were located at an intermediate point between the boundary and the nominal position assumed by the scaling of the boundary condition. In fact, the optimal virtual origin obtained by fitting the results of the wall-less simulations is not very far from the boundary plane itself. The reason for the offset was found to be the lack of correlation between the synthetic boundary and the overlying flow. In part because it is impossible to shrink a plane without also moving it and also because the boundary field has to be translated with respect to the reference one, to account for the mean shear, the reference and boundary planes quickly slide very far from each other. The reference plane only acts as a turbulence-like source from which to synthesize the boundary, and the results in this paper could probably have been obtained by using a reference plane from an unrelated simulation (Orlandi *et al.* 2003). That neglects the attached nature of the logarithmic-layer eddies (Townsend 1961), whose base is continually eroded. The wall-normal correlation length becomes very short at the numerical boundary, instead of remaining proportional to y, and the flow creates spurious small eddies whose sizes are closer to what should happen at the wall than to the interior of the logarithmic layer. The shear of the mean profile become steeper as the correlation length becomes smaller.

The last observation is significant, because most arguments for the logarithmic velocity profile rely on the correspondence between the length scale of the flow structures and the mean velocity gradient (Millikan 1938), which has often been interpreted to mean that the latter determines the former. The present result, where it is clear that the correlation length is artificially shortened by the procedure of generating the boundary condition, with the result of steepening the mean profile, proves that the opposite it true. It is the length scale of the structures that determines the profile.

Unfortunately, the previous remarks also imply that any off-wall boundary condition that attempts to reproduce the correct mean velocity profile must mimic the wall-normal correlation lengths, in addition to the in-plane ones scaled in the present study. How that can be achieved is not immediately obvious and is beyond the scope the present paper. This, as well as other extensions to enhance the applicability of the present boundary condition to practical cases, are currently under investigation.

Acknowledgements

This work was supported by the CYCIT grants TRA2006-08226, TRA2009-11498, the ERC advanced grant ERC-2010.AdG-20100224, and by allocations of computer time at the Barcelona Supercomputing Center. Y.M. was supported by the Spanish Ministry of Education and Science, under the Juan de la Cierva program, and by the SyeC Consolider Program CSD2007–00050. He was also partially supported by the Australian Research Council Discovery Projects funding scheme DP1095620. We are grateful to J. A. Sillero for the velocity correlations of the full-channel simulation in figure 8.

REFERENCES

ADRIAN, R. J. 2007 Hairpin vortex organization in wall turbulence. *Phys. Fluids* **19**, 041301.

ADRIAN, R. J., MAINHART, C. D. & TOMKINS, C. D. 2000 Vortex organization in the outer region of the turbulent boundary layer. *J. Fluid Mech.* **422**, 1–54.

https://doi.org/10.1017/jfm.2013.137 Published online by Cambridge University Press

DEL ÁLAMO, J. C. & JIMÉNEZ, J. 2009 Estimation of turbulent convection velocities and corrections to Taylor's approximation. *J. Fluid Mech.* **640**, 5–26.

DEL ÁLAMO, J. C., JIMÉNEZ, J., ZANDONADE, P. & MOSER, R. D. 2004 Scaling of the energy spectra of turbulent channels. *J. Fluid Mech.* **500**, 135–144.

DEL ÁLAMO, J. C., JIMÉNEZ, J., ZANDONADE, P. & MOSER, R. D. 2006 Self-similar vortex clusters in the turbulent logarithmic region. *J. Fluid Mech.* **561**, 329–358.

BAILEY, S. C. C., HULTMARK, M., SMITS, A. J. & SCHULTZ, M. P. 2008 Azimuthal structure of turbulence in high Reynolds number pipe flow. *J. Fluid Mech.* **615**, 121–138.

BAKKEN, O. M., KROGSTAD, P. A., ASHRAFIAN, A & ANDERSSON, H. I. 2005 Reynolds number effects in the outer layer of the turbulent flow in a channel with rough walls. *Phys. Fluids* **17**, 065101.

BULLOCK, K. J., COOPER, R. E. & ABERNATHY, F. H. 1978 Structural similarity in radial correlations and spectra of longitudinal velocity fluctuations in pipe flow. *J. Fluid Mech.* **88**, 585–608.

BUSCHMANN, M. H. & GAD-EL-HAK, M. 2005 New mixing-length approach for the mean velocity profile of turbulent boundary layers. *Trans. ASME: J. Fluids Engng* **127**, 393–396.

CATALANO, P., WANG, M., IACCARINO, G. & MOIN, P. 2003 Numerical simulation of the flow around a circular cylinder at high Reynolds numbers. *Intl J. Heat Fluid Flow* **24**, 453–469.

CHAMPAGNE, F. H., HARRIS, V. G. & CORRSIN, S. 1970 Experiments on nearly homogeneous turbulent shear flow. *J. Fluid Mech.* **41**, 81–139.

DEARDORFF, J. W. 1970 A numerical study of three-dimensional turbulent channel flow at large Reynolds numbers. *J. Fluid Mech.* **41**, 453–480.

DUNCAN, W. J., THOM, A. S. & YOUNG, A. D. 1970 *Mechanics of Fluids*, 2nd edn. Arnold.

FLORES, O. & JIMÉNEZ, J. 2006 Effect of wall-boundary disturbances on turbulent channel flows. *J. Fluid Mech.* **566**, 357–376.

FLORES, O., JIMÉNEZ, J. & DEL ÁLAMO, J. C. 2007 Vorticity organization in the outer layer of turbulent channels with disturbed walls. *J. Fluid Mech.* **591**, 145–154.

GUALA, M., HOMMEMA, S. E. & ADRIAN, R. J. 2006 Large-scale and very-large-scale motions in turbulent pipe flow. *J. Fluid Mech.* **554**, 521–542.

HAMBA, F. 2003 A hybrid RANS/LES simulation of turbulent channel flow. *Theor. Comput. Fluid Dyn.* **16**, 387–403.

HOYAS, S. & JIMÉNEZ, J. 2006 Scaling of velocity fluctuations in turbulent channels up to $Re_\tau = 2003$. *Phys. Fluids* **18**, 011702.

HOYAS, S. & JIMÉNEZ, J. 2008 Reynolds number effects on the Reynolds-stress budgets in turbulent channels. *Phys. Fluids* **20**, 101511.

HULTMARK, M., VALLIKIVI, M., BAILEY, S. C. C. & SMITS, A. J. 2012 Turbulent pipe flow at extreme Reynolds numbers. *Phys. Rev. Lett.* **108**, 094501.

HUNT, J. C. R., MOIN, P., MOSER, R. D. & SPALART, P. R. 1987 Self similarity of two point correlations in wall bounded turbulent flows. *CTR Annu. Res. Briefs*, 25–36.

HUNT, J. C. R. & MORRISON, J. F. 2000 Eddy structure in turbulent boundary layers. *Eur. J. Mech.* (B-*Fluids*) **19**, 673–694.

JIMÉNEZ, J. 1998 The largest scales of turbulent wall flows. *CTR Annu. Res. Briefs*, 137–154.

JIMÉNEZ, J. 2004 Turbulent flows over rough walls. *Annu. Rev. Fluid Mech.* **36**, 173–196.

JIMÉNEZ, J. 2007 Simulation of homogeneous and inhomogeneous shear turbulence. *CTR Annu. Res. Briefs*, 367–378.

JIMÉNEZ, J. 2012 Cascades in wall-bounded turbul.. *Annu. Rev. Fluid Mech.* **44**, 27–45.

JIMÉNEZ, J. & HOYAS, S. 2008 Turbulent fluctuations above the buffer layer of wall-bounded flows. *J. Fluid Mech.* **611**, 215–236.

JIMÉNEZ, J. & MOSER, R. D. 2000 LES: where are we and what can we expect?. *AIAA J.* **38**, 605–612.

KEATING, A. & PIOMELLI, U. 2006 A dynamic stochastic forcing method as a wall-layer model for large-eddy simulation. *J. Turbul.* **7**, N12.

KIM, K. C. & ADRIAN, R. J. 1999 Very large-scale motions in the outer layer. *Phys. Fluids* **11**, 417–422.

https://doi.org/10.1017/jfm.2013.137 Published online by Cambridge University Press

KIM, J., MOIN, P & MOSER, R. D. 1987 Turbulence statistics in fully developed channel flow at low Reynolds number. *J. Fluid Mech.* **177**, 133–166.

LOZANO-DURÁN, A., FLORES, O. & JIMÉNEZ, J. 2012 The three-dimensional structure of momentum transfer in turbulent channels. *J. Fluid Mech.* **694**, 100–130.

LUND, T. S., WU, X. & SQUIRES, K. D. 1998 Generation of turbulent inflow data for spatially-developing boundary layer simulations. *J. Computat. Phys.* **140**, 233–258.

MANSOUR, N. N., KIM, J. & MOIN, P. 1988 Reynolds-stress and dissipation-rate budgets in a turbulent channel flow. *J. Fluid Mech.* **194**, 15–44.

MILLIKAN, C. B. 1938 A critical discussion of turbulent flows in channels and circular tubes. In *Proceedings of 5th International Conference on Applied Mechanics*, pp. 386–392. Wiley.

MIZUNO, Y. & JIMÉNEZ, J. 2011 Mean velocity and length scales in the overlap region of wall-bounded turbulent flows. *Phys. Fluids* **23**, 085112.

MONTY, J. P., STEWART, J. A., WILLIAMS, R. C. & CHONG, M. S. 2007 Large-scale features in turbulent pipe and channel flows. *J. Fluid Mech.* **589**, 147–156.

MORRISON, W. R. B. & KRONAUER, R. E. 1969 Structure similarity for fully developed turbulence in smooth tubes. *J. Fluid Mech.* **39**, 117–141.

NIKITIN, N. V., NICOUD, F., EASISTHO, B., SQUIRES, K. D. & SPALART, P. R. 2000 An approach to wall modeling in large-eddy simulations. *Phys. Fluids* **12**, 1629–1632.

OBERLACK, M. 2001 Unified approach for symmetries in plane parallel shear flows. *J. Fluid Mech.* **427**, 299–328.

ORLANDI, P., LEONARDI, S., TUZI, R. & ANTONIA, R. A. 2003 Direct numerical simulations of turbulent channel flow with wall velocity disturbances. *Phys. Fluids* **15**, 3587–3601.

ÖSTERLUND, J. M., JOHANSSON, A. V., NAGIB, H. M. & HITES, M. 2000 A note on the overlap region in turbulent boundary layers. *Phys. Fluids* **12**, 1–4.

PASCARELLI, A., PIOMELLI, U. & CANDLER, G. V. 2000 Multi-block large-eddy simulations of turbulent boundary layers. *J. Comput. Phys.* **157**, 256–279.

PERRY, A. E. & ABELL, C. J. 1975 Scaling laws for pipe-flow turbulence. *J. Fluid Mech.* **67**, 257–271.

PERRY, A. E. & ABELL, C. J. 1977 Asymptotic similarity of turbulence structures in smooth- and rough-walled pipes. *J. Fluid Mech.* **79**, 785–799.

PIOMELLI, U. 2008 Wall-layer models for large-eddy simulations. *Prog. Aerosp. Sci.* **44**, 437–446.

PIOMELLI, U. & BALARAS, E. 2002 Wall-layer models for large-eddy simulations. *Annu. Rev. Fluid Mech.* **34**, 349–374.

PIOMELLI, U., BALARAS, E., PASINATO, H., SQUIRES, K. D. & SPALART, P. R. 2003 The inner/outer layer interface in large-eddy simulations with wall-layer models. *Intl J. Heat Fluid Flow* **24**, 538–550.

PODVIN, B. & FRAIGNEAU, Y. 2011 Synthetic wall boundary conditions for the direct numerical simulation of wall-bounded turbulence. *J. Turbul.* **12**, 1–26.

PUMIR, A. 1996 Turbulence in homogeneous shear flows. *Phys. Fluids* **8**, 3112–3127.

ROGERS, M. M. & MOIN, P. 1987 The structure of the vorticity field in homogeneous turbulent flows. *J. Fluid Mech.* **176**, 33–66.

SADDOUGHI, S. G. & VEERAVALI, S. V. 1994 Local isotropy in turbulent boundary layers at high Reynolds numbers. *J. Fluid Mech.* **268**, 333–372.

SCHUMANN, U. 1985 Algorithms for direct numerical simulation of shear-periodic turbulence. In *Ninth International Conference on Numerical Methods in Fluid Dynamics*, 218. Lecture Notes in Physics, pp. 492–496 Springer.

SIMENS, M. P., JIMÉNEZ, J., HOYAS, S. & MIZUNO, Y. 2009 A high-resolution code for turbulent boundary layers. *J. Comput. Phys.* **228**, 4218–4231.

SMAGORINSKY, J. 1963 General circulation experiments with the primitive equations I. The basic experiment. *Mon. Weath. Rev.* **91**, 99–164.

SMITS, A. J., MCKEON, B. J. & MARUSIC, I. 2011 High-Reynolds number wall turbulence. *Annu. Rev. Fluid Mech.* **43**, 353–375.

SPALART, P. R. 2009 Detached-eddy simulation. *Annu. Rev. Fluid Mech.* **41**, 181–202.

https://doi.org/10.1017/jfm.2013.137 Published online by Cambridge University Press

SPALART, P. R., COLEMAN, G. N. & JOHNSTONE, R. 2008 Direct numerical simulation of the Ekman layer: a step in Reynolds number, and cautious support for a log law with a shifted origin. *Phys. Fluids* **20**, 101507.

SPALART, P. R., MOSER, R. D. & ROGERS, M. M. 1991 Spectral methods for the Navier–Stokes equations with one infinite and two periodic directions. *J. Comput. Phys.* **96**, 297–324.

TENNEKES, H. & LUMLEY, J. L. 1972 *A First Course in Turbulence*. MIT.

TOMKINS, C. D. & ADRIAN, R. J. 2003 Spanwise structure and scale growth in turbulent boundary layers. *J. Fluid Mech.* **490**, 37–74.

TOWNSEND, A. A. 1961 Equilibrium layers and wall turbulence. *J. Fluid Mech.* **11**, 97–120.

TOWNSEND, A. A. 1976 *The Structure of Turbulent Shear Flow*, 2nd edn. Cambridge University Press.

WANG, M. & MOIN, P. 2002 Dynamic wall modeling for large-eddy simulation of complex turbulent flows. *Phys. Fluids* **14**, 2043–2051.

WOSNIK, M., CASTILLO, L. & GEORGE, W. K. 2000 A theory for turbulent pipe and channel flows. *J. Fluid Mech.* **421**, 115–145.

ZANOUN, E. S., DURST, F. & NAGIB, H. 2003 Evaluating the law of the wall in two-dimensional fully developed turbulent channel flows. *Phys. Fluids* **15**, 3079–3088.

https://doi.org/10.1017/jfm.2013.137 Published online by Cambridge University Press